Proceedings of GPPS Forum 18
Global Power and Propulsion Society
Zurich, 10th-12th January 2018
www.gpps.global

GPPS-2018-55

THE INFLUENCE OF INLET CORNER SHAPE ON THE STATIC AND DYNAMIC PERFORMANCE OF AN ANNULAR PRESSURE SEAL

Luis San Andrés
Mast-Childs Chair Professor
lsanandres@tamu.edu

Jing Yang[1]
Research Associate
yangjing@tamu.edu

Mechanical Engineering Dept., Texas A&M University, College Station, TX 77843, USA

ABSTRACT

Secondary flows thru annular seals in pumps must be minimized to improve their mechanical efficiency. Annular seals, in particular balance piston seals, also produce rotordynamic force coefficients which easily control the placement of rotor critical speeds and determine system stability. A uniform clearance annular seal produces a direct (centering) static stiffness as a result of the sudden entrance pressure drop at its inlet plane when the fluid flow accelerates from an upstream (stagnant) flow region into a narrow film land. This so called Lomakin effect equates the entrance pressure drop to the dynamic flow head through an empirical entrance pressure loss coefficient. Most seal designs regard the inlet as a sharp edge or square corner. In actuality, a customary manufacturing process could produce a rounded corner at the seal inlet. Furthermore, after a long period of operation, a sharp corner may wear out into a round section. Notice that to this date, bulk flow model (BFM) analyses rely on a hitherto unknown entrance pressure coefficient to deliver accurate predictions for seal force coefficients. This paper establishes the ground to quantify the influence of an inlet round corner on the performance of a water lubricated seal reproducing a configuration tested by Marquette et al. (1997). The smooth surface seal has clearance C_r = 0.11 mm, length L = 35 mm, and diameter D = 76 mm (L/D = 0.46). The test case considers a design operation at 10.2 krpm and 6.9 MPa pressure drop. Computational fluid dynamics (CFD) simulations apply to a seal with either a sharp edge or an inlet section with curvature r_c varying from ¼C_r to 5C_r. Note the largest radius (r_c) is just 1.6% of the seal length L. Going from a sharp edge inlet plane to one with a small curvature r_c = ¼C_r produces a ~20% decrease on the inlet pressure loss coefficient (ξ). A further reduction occurs with a larger circular corner; ξ drops from 0.43 to 0.17. That is, the entrance pressure loss will be lesser in a seal with a curved inlet. This can occur easily if the inlet edge wears due to solid particles eroding the seal inlet section. Further CFD simulations show that operating conditions in rotor speed and pressure drop do not affect the inlet loss coefficient, while the inlet circumferential swirl velocity does. In addition, an enlarged (double) clearance seal leads to an increase in the entrance pressure loss parameter as the inlet section becomes less round.

CFD predictions for most rotordynamic coefficients are within 10% relative to published test data, except for the direct damping coefficient C. For the seal with a rounded edge (r_c = 5 C_r) at the inlet plane, both the direct stiffness K and direct damping C decrease about 10% compared against the coefficients for the seal with a sharp inlet edge. The other force coefficients, namely cross-coupled stiffness and added mass, are unaffected by the inlet edge geometry. The same result holds for seal leakage, as expected. A BFM incorporates the CFD derived entrance pressure loss coefficients and produces rotordynamic coefficients for the same operating conditions. The CFD and BFM predictions are in good agreement, though there is still ~10% discrepancy for the direct stiffnesses delivered by the two methods. In the end, the analysis of the CFD results quantifies the pressure loss coefficient as a function of the inlet geometry for ready use in engineering BFM tools.

INTRODUCTION

A multistage centrifugal pump includes a variety of annular seals to limit secondary flows; for instance, neck ring seals, interstage seals, and balance piston seals. These seals can also provide rotor support and act as mechanical elements with stiffness and damping coefficients affecting the system rotordynamics. A balance piston seal can even control the placement of system critical speeds and influence its stability (Childs, 2013). An accurate evaluation of the static and dynamic performance of annular seals is thus imperative for the reliable operation of centrifugal pumps.

Figure 1 depicts the geometry of a typical annular seal, its nomenclature, and coordinate system for analysis. A liquid

[1] Corresponding author.

flows through the thin film annular region with clearance C_r between a stator and a rotor, whose diameter equals D, spinning with angular speed Ω. The fluid upstream of the seal is likely stagnant at supply pressure (P_s), fows through the seal film land length L, and exits the seal at ambient pressure (P_a) at $z = L$. At the seal inlet plane ($z = 0$), the fluid accelerates to produce a sudden pressure loss, from P_s to to P_e, largely determined by the evolving axial speed (W). The pressure drop (P_s-P_e) is a fluid inertia effect typically modeled as

$$(P_s - P_e) = \tfrac{1}{2}\, \rho\, (1 + \xi)\, W^2 \tag{1}$$

where ρ is the liquid density, W is the average axial velocity across the seal film, and ξ is a non-isentropic (empirical) pressure loss coefficient, likely a function of the geometry of the seal at its inlet plane. In Eq. (1), the larger ($1+\xi$) is, the lower the ratio (P_e/P_s) becomes, hence ξ acts as a significant flow resistance. Furthermore, the physical principle by which a direct stiffness (K) originates in an annular seal is due to this inertial pressure drop and its close interaction with the pressure drop (and flow resistance) within the seal film land. This *Lomakin effect*, known since the 1950's, affects the placement of critical speeds and sensitivity to rotor imbalance response in large pumps.

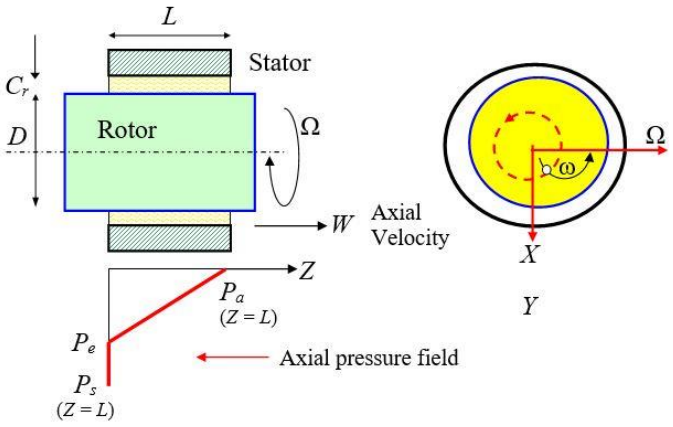

Fig. 1 Geometry of an annular pressure seal and coordinate system.

For small amplitude rotor displacements $\mathbf{x}=[x_{(t)},\ y_{(t)}]^{\mathrm{T}}$ along axes (X,Y), the fluid pressure field within the seal generates a reaction force, $\mathbf{F}=[F_X\ ,F_Y]^{\mathrm{T}}$, characterized by the linearized equation,

$$\begin{aligned} -\mathbf{F} &= -\begin{Bmatrix} F_X \\ F_Y \end{Bmatrix} = \mathbf{K}\,\mathbf{x} + \mathbf{C}\,\dot{\mathbf{x}} + \mathbf{M}\,\ddot{\mathbf{x}} \\ &= \begin{bmatrix} K_{XX} & K_{XY} \\ K_{YX} & K_{YY} \end{bmatrix} \begin{Bmatrix} x \\ y \end{Bmatrix} + \begin{bmatrix} C_{XX} & C_{XY} \\ C_{YX} & C_{YY} \end{bmatrix} \begin{Bmatrix} \dot{x} \\ \dot{y} \end{Bmatrix} + \begin{bmatrix} M_{XX} & M_{XY} \\ M_{YX} & M_{YY} \end{bmatrix} \begin{Bmatrix} \ddot{x} \\ \ddot{y} \end{Bmatrix} \end{aligned} \tag{2}$$

The matrices **K**, **C**, and **M** contain the (2×2) stiffness, damping and inertia force coefficients, respectively. Fluid inertia or added mass coefficients (**M**) are significant in seals with dense fluids operating at high surface speeds and with large pressure differentials. For an axisymmetric seal and rotor motions about a centered condition, the direct force coefficients are identical, whereas the cross-coupled coefficients are opposite in sign, i.e. $K_{XX} = K_{YY} = K$, and $K_{XY} = -K_{YX} = k$, for example.

The turbulent bulk-flow model (BFM), based on Hirs' lubrication theory (Hirs, 1973), is a common tool to predict the leakage, power loss, and rotordynamic force coefficients of annular seals. Examples abound as in (Childs, 2013; San Andrés, 1991) since a BFM implementation is straightforward and its immediate results are accurate compared to test data; in particular leakage and direct damping and inertia coefficients. The agreement for direct stiffness, however, is less compelling as the BFM requires an accurate estimation of the entrance pressure loss coefficient (ξ), see (Marquette et al., 1997; Al-Qutub et al., 2000).

Head or pressure losses in flows through sudden changes in pipe cross-section have an immense importance in engineering work and applications. Investigations abound to encompass both experimental and analytical validations. Benedict et al. (1966) in the mid 1960's review the empirical equations for estimation of head loss coefficients, as a fraction of the dynamic pressure head, for flows with incompressible and compressible fluids thru sudden pipe section enlargements and contractions. For a constant density fluid flow, turbulent in character, the loss coefficient is determined by the ratio of pipe diameters (upstream/downstream), whereas for a compressible fluid, the loss parameter is also affected by the ratio of total pressures (inlet/outlet), and the fluid properties. In short, the larger the change in pipe diameter, the larger the head loss coefficient. Later, Bullen et al. (1987) demonstrate the head loss coefficient also depends on the Reynolds number for turbulent flows with an incompressible fluid, and while emphasizing that the sharpness of the contraction has a significant influence on the pressure loss.

In a Rayleigh-step fluid film bearing, there is a sudden pressure loss at the geometrical discontinuity. Constantinescu and Galetuse (1976) first included the fluid inertia effect in lubrication theory and derived an entrance loss coefficient that depends on the ratio of film thicknesses and the magnitude of the shear flow velocity (Reynolds number). $\xi \sim 0.10$-0.20 for steps with a large thickness ratio (upstream/downstream) and turbulent flow. The authors also note that for a too small film thickness, a pressure rise rather than a pressure drop happens at the steep interface. Similarly, San Andrés and Velthuis (1992), in a program contemplating hybrid bearings for cryogenic turbo pumps, performed 2D flow simulations to obtain the entrance pressure loss coefficient (ξ) at the sharp edges of a hydrostatic pocket. San Andrés and Velthuis (1992) states $\xi = 0.7$ for pressure induce flow and $\xi = 0.6$ for shear induced flow.

As to the entrance pressure loss coefficient for the liquid annular pressure seals, Childs (2013) summarizes empirical estimations of ξ varying from 0.1 to 0.5. Marquette et al. (1997) recommend ξ=0.10 for low inlet pre-swirl. Other authors use ξ=0.25, a magnitude derived from matching the predicted flow rate to one known test condition (San Andrés, 1991). In many other instances, authors simply use someone else's ξ, without justification. Needless to say, both accurate

inlet loss coefficient (ξ) and a wall shear stress model influence the precision prediction delivered by a BFM tool.

With the rapid development of computer technology, CFD is becoming a routine engineering tool for the performance analysis of pump seals. Ha and Choe (2012) employ CFD software to investigate the leakage and rotordynamic coefficients of a water lubricated eccentric annular seal in Marquette et al. (1997). The CFD predictions are closer to the test data for direct stiffness and damping coefficients than results by the BFM.

However, CFD analyses still demand of a long computational time compared with the expediency of a BFM. A hybrid CFD-BFM approach is a meaningful development direction that combines the accuracy of CFD with the practicality of a BFM, while reducing the excessive computation time for (multiple) CFD unsteady flow simulations required for evaluation of force coefficients. Prominent on the engineering implementation of these hybrid methods are the works of Arghir and Frene (2004), Migliorini et al. (2013) and San Andrés et al. (2017) whom extract wall shear stresses from steady CFD results and fit them to Blasius friction factors formulas for immediate implementation in a BFM predictive tool.

Aiming to improve the prediction of seal dynamic force coefficients, Grigoriev et al. (2006) recognize the need of an accurate entrance pressure loss coefficient (ξ) for ready use with a BFM tool. The authors completed two-dimensional CFD (steady flow) simulations of a smooth surface gas seal (L/D=0.34) and modeled ξ as a function of the local seal clearance. With the aid of the numerically found ξ, the BFM delivers accurate stiffness coefficients for a honeycomb seal when compared to test data in (Elrod et al., 1990). Prior BFM predictions showed large difference (> 100%) with the test results. However, the derived ξ is as large as 1.23. Importantly enough, in tests with a gas seal of uniform clearance, Al-Qutub et al. (2000) report an empirical ξ that is independent of either the inlet flow Mach number (<0.5) or the axial flow Reynolds number or the seal clearance. In (Al-Qutub et al., 2000), ξ =0.70 for a uniform clearance (smooth surface) seal, whereas ξ = 1.08 for a honeycomb seal. The dissimilar magnitudes in published ξ attest to not just the complexity of the flow field but also the myriad of service conditions typical seals must undergo.

Note that most analyses (and practice) consider the seal inlet to have a sharp edge (or square corner). In actuality an inaccurate manufacturing process could produce a rounded corner, as shown in Figure 2. The figure displays the seal inlet section with either rectangular corner or a circular corner with radius $r_c \sim C_r$, of the same size as C_r, the seal clearance. Due to manufacturing poor tolerances, the inlet corner shape of a seal may deviate from a sharp edge. Furthermore, after a period of operation, a sharp corner in an annular seal may wear out into a round corner. The variation of the inlet corner shape also influences the pressure drop at the seal entrance, which results in the uncertainties of entrance loss coefficient and the seal direct stiffness.

The present work is a concerted effort to investigate the influence of the rounded inlet corner on annular seal leakage, static pressure distribution, and rotordynamic force coefficients. CFD simulations apply to a water lubricated annular pressure seal with either a sharp edge or an inlet with curvature radius r_c = ¼, ½, 1, 2, 3, 4, 5 C_r. The research addresses the effects of a seal inlet round corner, inlet swirl ratio, rotor angular speed, and a two-fold nominal clearance emulating a worn seal on the seal leakage and entrance pressure drop, as well as the exit circumferential flow velocity. The influence of the inlet corner shape on the rotordynamic force coefficients is also considered.

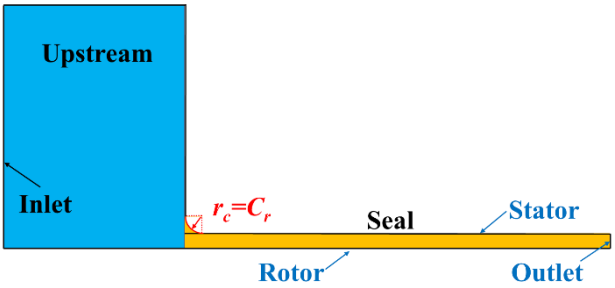

Fig. 2 Schematic diagram of seal inlet plane with either a square or a round corner (not to scale).

NUMERICAL METHODS

Seal geometry and operating conditions

To evaluate the influence of an inlet round corner on the static and rotordynamic performance of an annular seal with uniform clearance and smooth stator and rotor surfaces, the present work employs a water lubricated test seal detailed in Marquette et al. (1997). Table 1 lists the seal geometry, operating condition and fluid properties, respectively. The seal with an inlet round corner is semi-circular in shape, just as Figure 2 displays. Except for the inlet corner shape, either sharp edge or round, all other parameters are identical. Note $L/C_r \sim 317$; hence, even with a large round corner $r_c = 5C_r$, the section with a round inlet represents a minute fraction of the seal length. That is, L/r_c = 63.5 for the circular corner with largest radius.

Table 1. Geometry of smooth surface annular seal and operating conditions. Taken from Marquette et al. (1997).

Rotor radius, R	38.15 mm
Seal length, L	34.93 mm
Clearance, C_r	0.11 mm
Pressure difference, ΔP	6.89 MPa
Rotor speed, Ω	10,200 rpm
Surface speed, ΩR	40.77 m/s
Inlet swirl ratio, α	0.0
Whirl orbit radius, r	0.10 C_r
Fluid	water
Density, ρ	998 kg/m^3
Kinematic viscosity, ν	1.14×10^{-6} m^2/s
Corner radius, r_c / C_r	0, ¼, ½, 1, 2, 3, 4, 5

Computational grids

Since the smooth annular pressure seal is axisymmetric, a numerical simulation of two-dimensional flow through the seal is efficient to obtain its steady flow performance. The flow domain region, as shown in Fig. 3, comprises of an upstream section or inlet plenum where the fluid is nearly stagnant and a thin film land section with length L and clearance C_r. Note, as shown in Fig. 3, the seal proper section (film land) is a fraction of the flow domain. To capture precisely the seal steady-state flow characteristics, in particular with a round inlet corner, a first step proceeds to determine the adequate length (L_u) and width (w_u) of the upstream section. This preliminary work, not presented herein for brevity, set the proper mesh size and density. In sum, the results prove that L_u=w_u = ¼ L or longer. In the following, the flow domain includes an upstream section with L_u=w_u = ¼ L. Figure 3 displays the mesh with 1.3×10^4 nodes for the seal upstream section with L_u=w_u = ¼ L and an inlet round corner with r_c = ½ C_r.

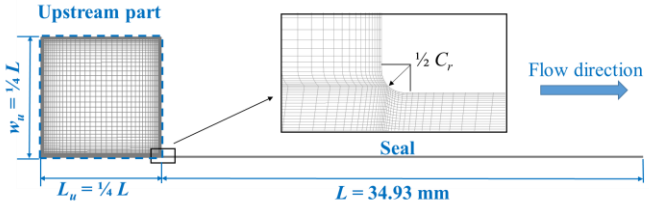

Fig. 3 View of mesh for two-dimensional flow in an annular seal. Seal with an inlet round corner (r_c = ½ C_r). Upstream flow section with length and width L_u = w_u = ¼ L shown. Inset showcases mesh density at inlet section of seal land.

Solution methods

A commercial CFD software (ANSYS, 2013) solves the Reynolds-Averaged Navier-Stokes equation. The turbulence flow model is a standard k-ε model with a scalable wall function. The pressure at the seal inlet (upstream section) and outlet are set as 6.89 MPa and 0, respectively. The no-slip fluid velocity condition applies to the rotor and stator surfaces. Note the circumferential speed of the fluid is set as zero at z=-L_u, except at the bottom wall that represents the spinning rotor with surface speed (ΩR).

To evaluate the seal rotordynamic force coefficients, the rotor whirls with a circular centered orbit with frequency (ω) and amplitude (r), as depicted in Fig. 4. Note that the flow field appears steady in a rotating coordinate frame ($\bar{X},\bar{Y}$) that turns with the whirl frequency. To reproduce this condition, a steady flow CFD model considers the stator spins with speed $-\omega$, and the rotor is *eccentric* with offset r while turning with angular speed (Ω-ω). The change to a moving reference frame avoids using a complex *moving* (distorted) mesh.

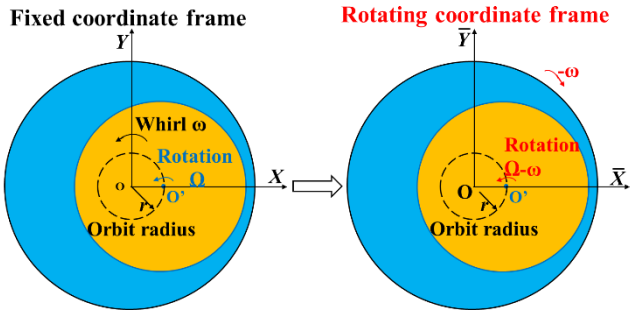

Fig. 4 Schematic view of rotor spinning with angular speed Ω and orbiting about its center with amplitude r and whirl frequency ω (not to scale). Fixed coordinates (X,Y) & rotating coordinates ($\bar{X},\bar{Y}$).

RESULTS AND DISCUSSION

Presently, numerous CFD simulations of the flow in an annular seal are performed to quantify the effects of

(a) seal inlet round corner,
(b) inlet circumferential swirl speed,
(c) rotor angular speed and pressure drop, and
(d) a two-fold nominal clearance emulating a worn seal

on the leakage ($\dot{m}$), entrance pressure (P_e), and inlet and exit circumferential flow velocities (U_θ). From these results, an accurate estimation of the entrance pressure loss coefficient (ξ) follows. The influence of the inlet corner shape on the seal rotordynamic force coefficients is shown at the end.

Effect of an inlet round corner on seal leakage and entrance pressure loss coefficient

Table 2 lists the predicted seal leakage or mass flow rate ($\dot{m}$), entrance pressure ratio (P_e/P_s), and inlet pressure loss coefficient (ξ) for the various seal inlet round corners considered. The magnitudes atop the table show the leakage and average axial velocity (W) for the seal with a sharp corner (square edge) and hereby referred as baseline parameters. Marquette et al. (1997) reports a measured $\dot{m}$ =1.09 kg/s, while the leakage for the seal with a sharp edge is 1.12 kg/s (just 3 % higher). The table shows a percent variation of the leakage and mean flow axial velocity from the baseline condition. With a round inlet corner, the leakage slightly increases (6%) relative to the flow in a seal with a sharp inlet edge, a result of the slight increment in seal inlet area. The variation in W for the seal with a sharp edge towards that with a round corner shows a similar trend, +4.1%.

The swirl ratio $\alpha = U_\theta/(\Omega R)$ equals the mean flow circumferential fluid velocity (across the clearance) divided by the rotor surface speed (ΩR). The table notes both inlet and exit swirl ratios, α_{in} and α_e, are identical for the seal with either a sharp corner or a round corner. Recall the fluid circumferential speed is set to zero at the beginning of the upstream section (z = -L_u); nonetheless the fluid begins to swirl, drawn by the spinning rotor, so that at the seal inlet (z = 0), α_{in} ~ =0.13, i.e., 13% of surface speed. The result is in opposition to conventional BFM assumptions.

The seal inlet section (sharp or round) has little effect on either the leakage ($\dot{m}$) or the mean flow axial velocity (W), recall $\dot{m} = \rho\ \pi\ D\ C_r\ W$. Presently, the wall shear stresses along the seal land, i.e. $L/C_r >> 1$, affect most $\dot{m}$. Incidentally, for a seal with a round corner, P_e and W are obtained at the location where the inlet plane curvature ends. Going from a sharp edge inlet plane to one with a small radius of curvature r_c = ¼ C_r produces a decrease of the entrance pressure loss coefficient (ξ) from 0.54 to 0.43, a reduction of ~20%. A further reduction occurs with a larger circular corner, ξ = 0.37 for r_c = ¼ C_r to ξ = 0.17 for r_c =5 C_r. That is, ξ is lesser in a seal with a curved inlet. This can occur easily if the inlet edge wears due to solid particles (in water) eroding the inlet section of the seal.

Table 2. CFD predicted leakage, axial flow velocity, entrance pressure (P_e), and loss coefficient (ξ) for seal with an inlet section as a sharp corner or a round corner with increasing curvature.

Leakage $\dot{m}$ =1.12 kg/s, average axial velocity W=43.46 m/s
Inlet swirl ratio α_{in} = 0.13, outlet swirl ratio α_{in} = 0.49

	r_c	$\Delta\dot{m}$ [%]	ΔW [%]	P_e/P_s	ξ
Sharp corner	0	0	0	0.789	0.54
Circular shape corner	¼ C_r	+2.2	+0.03	0.803	0.43
	½ C_r	+2.8	+1.4	0.807	0.37
	1 C_r	+3.7	+2.1	0.813	0.31
	2 C_r	+4.6	+2.7	0.821	0.24
	3 C_r	+5.2	+3.2	0.824	0.21
	4 C_r	+5.7	+3.6	0.826	0.18
	5 C_r	+6.0	+4.1	0.827	0.17

(L/D=0.46, C_r = 0.11 mm, ΔP= 6.89 MPa and 10. 2 krpm).

Figure 5 displays the static pressure acting on the rotor surface along the axial direction. The graphs display predictions for the sharp (rectangular shape) edge and a rounded shape corner with r_c = ¼ C_r and r_c = 5C_r. The round corner reduces the sharp drop of static pressure near the seal entrance. The variation of the inlet shape from a sharp edge to a round edge, even one with a small radius r_c = ¼ C_r, has a significant influence on the static pressure distribution near the seal entrance plane (z=0), and which will also influence the generation of direct stiffness (K), as shown later. Figure 5(b) is a zoom section near the seal entrance plane. For the seal with the largest round corner (r_c = 5C_r), the pressure gradually decreases along the curvature, i.e. from seal entrance (z = 0) till 5C_r (z = 0.55 mm).

To further understand the static pressure variation near the seal entrance, Figure 6 displays the pressure contours near the seal entrance for a cut-plane of the seal with (a) a sharp edge and (b) a circular corner (r_c = C_r). The pressure decreases more after entering the film land for the seal land with a square corner. There is also a low-pressure area near the stator surface at the seal entrance. While for the seal with a circular inlet corner, the pressure decreases smoothly around the corner. Figure 7 shows the streamlines distribution around the seal with a sharp corner and with a circular corner (r_c = C_r), respectively. As to the annular seal with square corner, a small recirculation region (vena contracta) appears near the stator, in accordance with the low-pressure section displayed in Figure 6(a). The axial velocity profile depicts evidences a region of back flow near the stator wall.

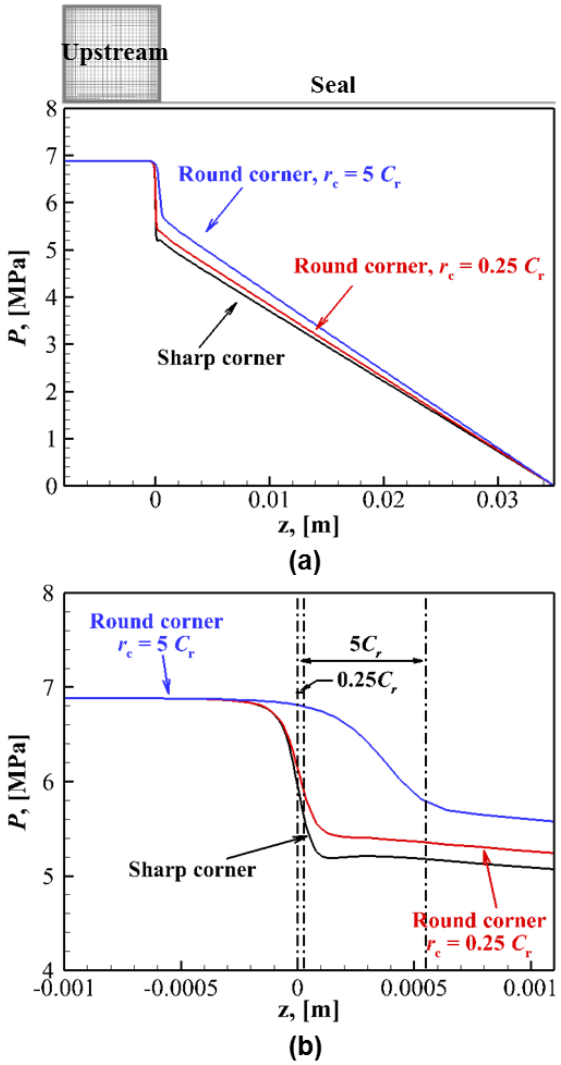

Water lubricated seal: 6.89 MPa pressure drop and rotor speed of 10,200 rpm.

Fig. 5 Predicted static pressure [MPa] on rotor surface vs. axial direction z [m], for annular seal with a square corner or a round corner (r_c = ¼C_r and 5C_r). (a) Distribution from upstream section to seal exit plane; (b) distribution near seal entrance plane.

Effect of inlet circumferential swirl on seal leakage and entrance pressure loss coefficient

The inlet circumferential speed (or swirl ratio α_{in}) has an impact on the seal rotordynamic force coefficients. Presently CFD simulations model the seal with length (L/D=0.46), with either a sharp edge or a round corner (r_c = 5C_r) at the inlet, and an inlet swirl ratio α_{in}= -0.5 or 1.0. The seal geometry and other operating conditions remain invariant.

Table 3 sums the predictions of seal leakage, entrance pressure ratio (P_e/P_s), and entrance pressure loss coefficient (ξ) for two inlet shape configurations, a sharp edge and a

round one. Changes in α_{in} have a small influence on both seal leakage, average axial velocity, and entrance pressure. Note the exit circumferential velocity approaches 50% of the rotor surface speed, $\alpha_{out} \rightarrow$ ½, irrespective of the inlet swirl as the seal is long. Relative to the case with α_{in}=0.13, ξ for a sharp edge inlet increases by 10% or more with α_{in}=-0.5 or 1. The entrance pressure loss coefficient ξ for the round edge seal is a small fraction of the one for a sharp edge at the seal inlet, though it increases for the incoming flow swirling with α_{in}=-0.5 or 1; the change is larger for the case with largest inlet swirl.

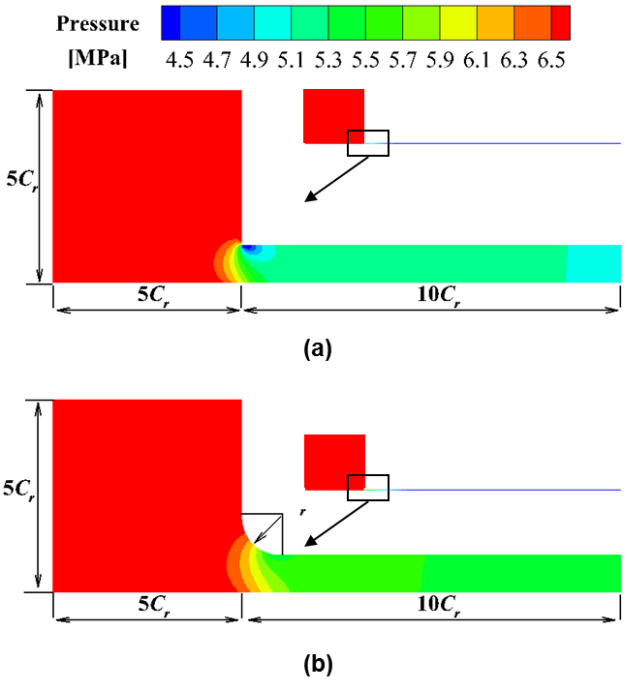

Seal (L/D = 0.46), 6.89 MPa pressure drop and speed 10.2 krpm

Fig. 6 Pressure contours [MPa] around seal entrance with (a) a square corner or (b) a round corner (r_c = C_r).

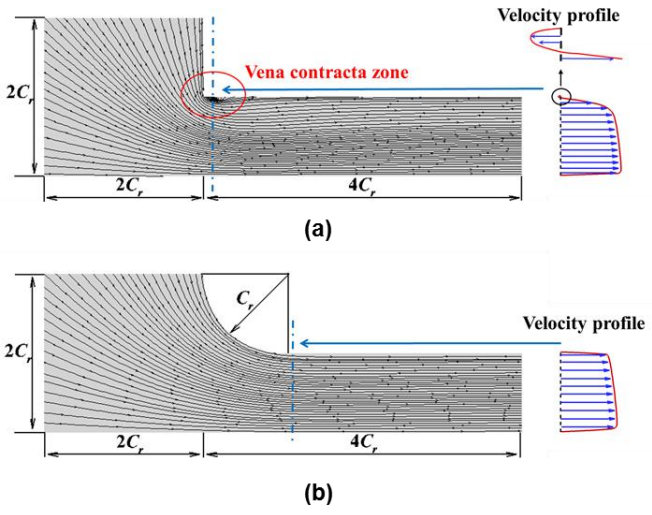

Seal (L/D = 0.46), 6.89 MPa pressure drop and speed 10.2 krpm

Fig. 7 Streamlines near seal entrance plane with (a) a sharp edge or (b) a circular corner (r_c = C_r).

Table 3. CFD predicted leakage, axial flow velocity, entrance pressure (P_e), and loss coefficient (ξ) for seal with an inlet section as a sharp corner or a round corner (r_c = 5C_r). Inlet swirl (α_{in}) condition varies.

Leakage $\dot{m}$ =1.11 kg/s, average axial velocity W=43.46 m/s, outlet swirl ratio α_{out} = 0.49

	$\Delta\dot{m}$ [%]	ΔW [%]	α_{in}	P_e/P_s	ξ	$\Delta\alpha_{out}$ [%]
Sharp corner	-0.1	-0.2	- ½	0.789	0.60	-1.2
	0	0	0.13	0.789	0.54	0
	+0.06	+0.09	1.0	0.773	0.70	+1.2
Round corner (r_c=5C_r)	+5.8	+3.8	- ½	0.828	0.21	-1.7
	+6.0	+4.1	0.13	0.827	0.17	-0.5
	+6.2	+4.2	1.0	0.814	0.29	+0.9

(L/D = 0.46, C_r = 0.11 mm, ΔP= 6.89 MPa and 10. 2 krpm)

Effect of rotor angular speed on seal leakage and entrance pressure loss coefficient

A further investigation applies to the annular seal (L/D=0.46) operating at two other shaft speeds, above and below the design condition of Ω=10 krpm. The examples are $\Omega_1 = 0.75\times\Omega = 7.65$ krpm and $\Omega_2 = 1.25\times\Omega = 12.75$ krpm. In a pump, the pressure drop $\Delta P \sim \Omega^2$, hence the seal operates with $\Delta P_1 = 0.75^2\times\Delta P$= 3.86 MPa and $\Delta P_2 = 1.25^2\times\Delta P$= 10.77 MPa, respectively.

Table 4 lists the CFD predictions for a seal with an inlet as a sharp edge or one with a rounded corner r_c = 5 C_r. As expected, the leakage is proportional to shaft speed ($Q = \dot{m}/\rho \sim \Delta P^{1/2} \sim \Omega$,). The average axial velocity changes in accordance with the leakage. Both inlet and exit swirl velocity ratios remain independent of shaft speed (or pressure drop). Most importantly, the entrance pressure loss coefficient (ξ) does hardly change with the operating flow condition (ΔP or Ω) , albeit the seal inlet edge shape makes apparent distinct magnitudes.

Table 4. CFD predicted leakage, axial flow velocity, entrance pressure (P_e), and loss coefficient (ξ) for seal with an inlet section as a sharp corner or a round corner (r_c = 5C_r). Operation at three shaft speeds and pressure drop $\Delta P \sim \Omega^2$.

Inlet swirl ratio α_{in} = 0.13, outlet swirl ratio α_{in} = 0.49.

	speed [rpm]	ΔP [MPa]	$\dot{m}$ [kg/s]	W [m/s]	P_e/P_s	ξ
Sharp corner	7,650	3.86	0.82	31.81	0.798	0.55
	10,200	6.89	1.12	43.46	0.789	0.54
	12,750	10.75	1.43	55.45	0.780	0.54
Round corner (r_c=5C_r)	7,650	3.86	0.87	33.05	0.836	0.17
	10,200	6.89	1.19	45.23	0.827	0.17
	12,750	10.75	1.52	57.81	0.820	0.16

As a note, the axial Reynolds number $\mathrm{Re}_a = 2\rho W C_r/\mu \approx 6{,}143$ and the circumferential Reynolds number $\mathrm{Re}_c = 2\rho\Omega R C_r/\mu \approx 5{,}900$ for the seal operating at the lowest speed (Ω_1). The flow remains turbulent thru the seal land length.

Effect of a worn clearance on seal leakage and entrance pressure loss coefficient

All pump seal surfaces wear out. Hence, consider the seal in Table 1 (with an inlet sharp edge or one with a round corner with $r_c = 5C_r$) wears out so that its clearance doubles (C_{r2} = 0.22 mm). For the seal with a round corner, the bottom parts of its curvature wears into a flat section extending slightly its film land length. Table 5 sums the results of the CFD analysis predictions. For the seal with a round edge, the flow parameters (P_e and W) are determined at the location where the curvature of the inlet plane ends. Seal leakage increases significantly with a two fold increase in clearance, thus diminishing the seal ability to restrict flow. For the seal with a double size clearance, the average axial velocity increases ~ 36% relative to that with nominal clearance. The entrance pressure loss coefficient for a sharp edge seal changes little as the seal clearance doubles ($\xi \sim 0.54$). Not so for the round edge seal which evidences a dramatic increase $\xi = 0.17 \rightarrow 0.32$ since the inlet corner curvature is less pronounced as the clearance increases. For the nominal clearance seal, refer to Table 2 ξ obtained with $r_c < 4\ C_r$. Note also the entrance pressure drop (P_e/P_s) decreases as the clearance doubles since the axial flow is much larger.

Table 5. CFD predicted leakage, axial flow velocity, entrance pressure (P_e), and loss coefficient (ξ) for seal with an inlet section as a sharp corner or a round corner ($r_c = 5C_r$). Seal with nominal clearance C_r and double clearance C_{r2} = 0.22 mm

Inlet swirl ratio α_{in} = 0.13, outlet swirl ratio α_{in} = 0.49.

	Clearance	$\dot{m}$ [kg/s]	W [m/s]	P_e/P_s	ξ
Sharp corner	C_r	1.12	43.46	0.789	0.54
	2 C_r	3.08	59.01	0.609	0.55
Round corner (r_c = 5 C_r)	C_r	1.19	45.23	0.827	0.17
	2 C_r	3.26	61.21	0.642	0.32

(ΔP= 6.89 MPa and 10,200 rpm rotor speed).

The sum of the knowledge acquired thru the CFD results follows. Figure 8 depicts the entrance pressure loss coefficient (ξ) versus the curvature of the inlet edge for the various seal conditions in geometry and operation discussed above. It is evident that ξ changes most (rapidly) as soon as the curvature of the inlet section departs from a sharp (square) edge. The largest inlet curvature (r_c= 5C_r,) produces the lowest ξ. Seal clearance affects little ξ for the sharp edge seal; whereas it affects most ξ for a seal with a large inlet curvature. Seal operating conditions (speed and pressure drop) do not affect ξ, alas the inlet circumferential swirl velocity does. In brief, the entrance pressure loss coefficient is a remarkable function of the seal inlet edge configuration.

The influence of an inlet round corner on the seal rotordynamic force coefficients

One three-dimensional mesh, node count ~ 3.1×10^6, is produced for estimation of the seal rotordynamic force coefficients. A grid independence analysis proves this mesh is fine enough to capture the flow details in the seal studied.

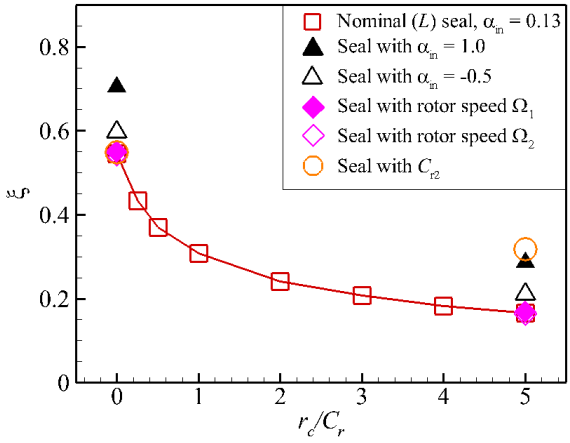

Fig. 8 CFD derived entrance pressure loss coefficient (ξ) vs. corner radius for seal with nominal length (L), *a* seal with inlet swirl ratio equalling to 1.0 or -0.5, a seal with rotor speed Ω_1 or Ω_2, and a seal with a two-fold clearance.

Recall the three-dimensional flow field appears steady in the rotating reference frame ($\bar{X}, \bar{Y}$), as shown in Figure 4. In the CFD analyses, the rotor angular speed (Ω) is 10,200 rpm whereas the whirl frequency (ω) increases from -4,800 to 14,400 rpm ($-0.47 < \omega/\Omega < 1.41$). The orbit radius or rotor dynamic eccentricity r= 0.1 C_r. For each excitation frequency ω_i, the radial and tangential components $\left(F_{\bar{X}}, F_{\bar{Y}}\right)_{i=1,N}$ of the seal reaction force are evaluated from integration of the calculated pressure field on the rotor surface. Next, curve fittings apply to the set ($F_{\bar{X}}/r$ and $F_{\bar{Y}}/r)_i$ for estimation of the rotordynamic force coefficients. That is,

$$- F_{\bar{X}}/r \leftarrow K + \omega c - \omega^2 M; \; - F_{\bar{Y}}/r \leftarrow -k + \omega C \qquad (3)$$

From these coefficients, it is usual to calculate the seal whirl frequency ratio, WFR=$k/(C\Omega)$, a most useful parameter denoting the seal ability to contribute to the stability (or not) of a rotating system.

Figure 9 displays the seal radial and tangential forces, ($F_{\bar{X}}/r$) and ($F_{\bar{Y}}/r$), versus frequency (ω) for a seal with an entrance plane as a sharp edge or one with curvature (r_c) increasing from ¼C_r to 5C_r. The solid lines represent constructed from the test data in Marquette et al. (1997). The dashed lines are the curve fittings to the CFD predictions; the correlation coefficient $R^2 > 0.93$ for all curves. For a round inlet corner the radial force ($F_{\bar{X}}/r$) decreases in magnitude with an increase in corner radius, and hence the seal produces a lesser static stiffness (K), as the intersection at $\omega = 0$ reveals. The slope for tangential force ($F_{\bar{Y}}/r$) decreases as the radius of the round corner increases, hence the direct damping coefficient (C) decreases. The results for the seal with round corner r_c / C_r = 2, 3 and 4 are not displayed in Figure 9 for clarity.

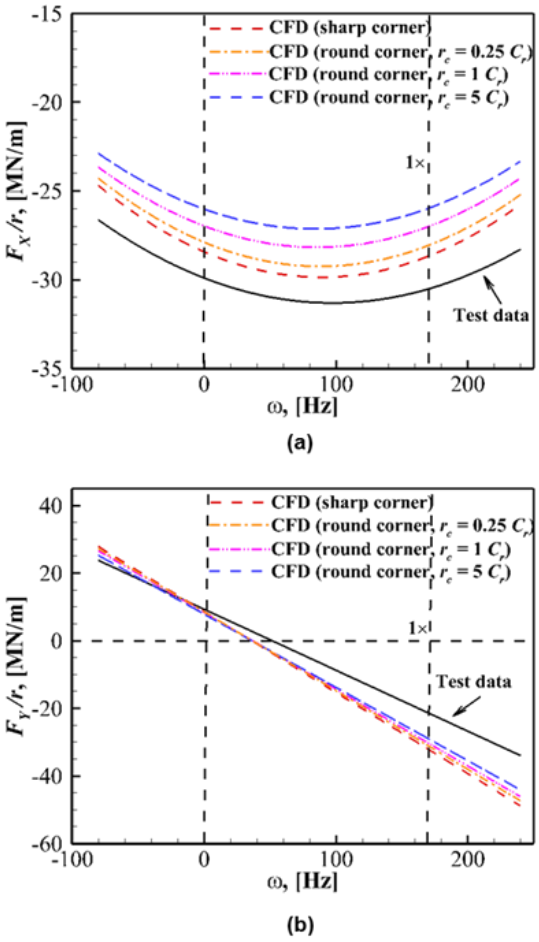

Fig. 9 Components of seal reaction force (radial and tangential) $(F_{\bar{X}}, F_{\bar{Y}})/r$ vs. excitation frequency ω. Effect of inlet corner shape (sharp to round). Water seal (L/D=0.46): 6.89 MPa pressure drop and rotor speed of 10.2 krpm. Test data from Marquette et al. (1997).

Figure 10 shows the CFD predicted rotordynamic force coefficients versus (r_c/C_r) for the seal with geometry and operating conditions in Table 1. In the graphs, r_c/C_r =0 denotes the annular seal with a sharp inlet corner. The graphs also include test results from Marquette et al. (1997) for a seal with a sharp corner, and the numerical predictions delivered by a bulk-flow model (San Andrés, 1991). Bars denote the uncertainty for the test data. Since the BFM does not consider the effect of the seal inlet plane shape, the entrance pressure loss coefficient obtained by CFD is used for predictions. Other operating conditions for the BFM are identical to those listed in Table 1.

As for the seal with a sharp edge at the inlet plane, the CFD predictions are good for most rotordynamic coefficients (within 10% differences with the test data (Marquette et al., 1997)), except for the direct damping coefficient C. The CFD model over predicts C by 33% larger than the test data. For the seal with a rounded edge (r_c = 5 C_r) at the inlet plane, both the direct stiffness K and direct damping C decrease about 10% when compared against the coefficients for the seal with a sharp inlet edge. The other rotordynamic coefficients appear invariant. Due to the relatively smooth decrease of the static pressure near the seal entrance, the direct stiffness K is (as expected) lower for the seal with a circular (round) corner. The rotordynamic coefficients predicted by the BFM show similar trends as those from the CFD analysis, respectively. The direct stiffness K and direct damping C decrease as the edge transits from a sharp inlet edge to one with a round corner. The cross-coupled stiffness k, cross-coupled damping c, and inertia M also slightly decrease.

CONCLUSION

The inlet corner shape of an annular pressure seal can deviate from a designed sharp edge due to a manufacturing uncertainty or wearing out after a period of operation. Variations on the shape of the inlet plane of a seal, sharp or round, can have an impact of the seal entrance pressure and swirl velocity, and most importantly, on the generation of a centering stiffness. The CFD analysis considers a water lubricated, smooth surface seal (L/D = 0.46) with either a sharp edge or a circular corner with radius r_c increasing from ¼ to 5 C_r. The analysis considers also changes in the inlet swirl ratio, rotor speed and pressure drop, and an enlarged clearance due to wear. The authors (Yang and San Andrés, 2018) offer a further example, including a variation in seal length as well as a study on the mesh sensitivity to produce accurate results.

The CFD predictions demonstrate that the entrance pressure loss coefficient (ξ) decreases rapidly as soon as the curvature of the inlet section departs from a sharp edge; the larges inlet curvature (r_c= 5 C_r) produces the lowest ξ. The influence of seal clearance on ξ is small for the sharp edge seal, whereas the clearance affects ξ most for a seal with a large inlet curvature. Seal operating conditions (rotor angular speed and pressure drop) have no influence on ξ, while the inlet circumferential swirl velocity does.

Going from a sharp edge towards a round corner, the direct stiffness K and direct damping C of the annular pressure seal decrease. For the seal with a round corner (r_c = 5 C_r) at the inlet, both the direct stiffness K and direct damping C decrease about 10% compared with the coefficients for the seal with a sharp inlet edge. The other rotordynamic coefficients decrease only slightly. For a seal with an inlet round corner of increasing radius (r_c > 2 C_r), the variation for all the rotordynamic coefficients is minute.

The analysis of the CFD results explains how a rounded inlet corner influences the inlet loss coefficient and direct stiffness of an annular seal. The results also provide a direction for the consideration of an inlet corner shape in a bulk flow mode (BFM) analysis. With the inlet loss coefficient provided by CFD, the BFM performs better albeit its predictions are persistently smaller than those from the CFD analysis and when compared to test results.

Both an inlet sharp edge and a round edge, either a result from manufacturing or wear from use, have no remarkable effect on seal leakage and only a minor influence on the seal direct stiffness. The entrance loss coefficient presented herein, however, is crucial for the estimation of seal stiffness using a BFM analysis.

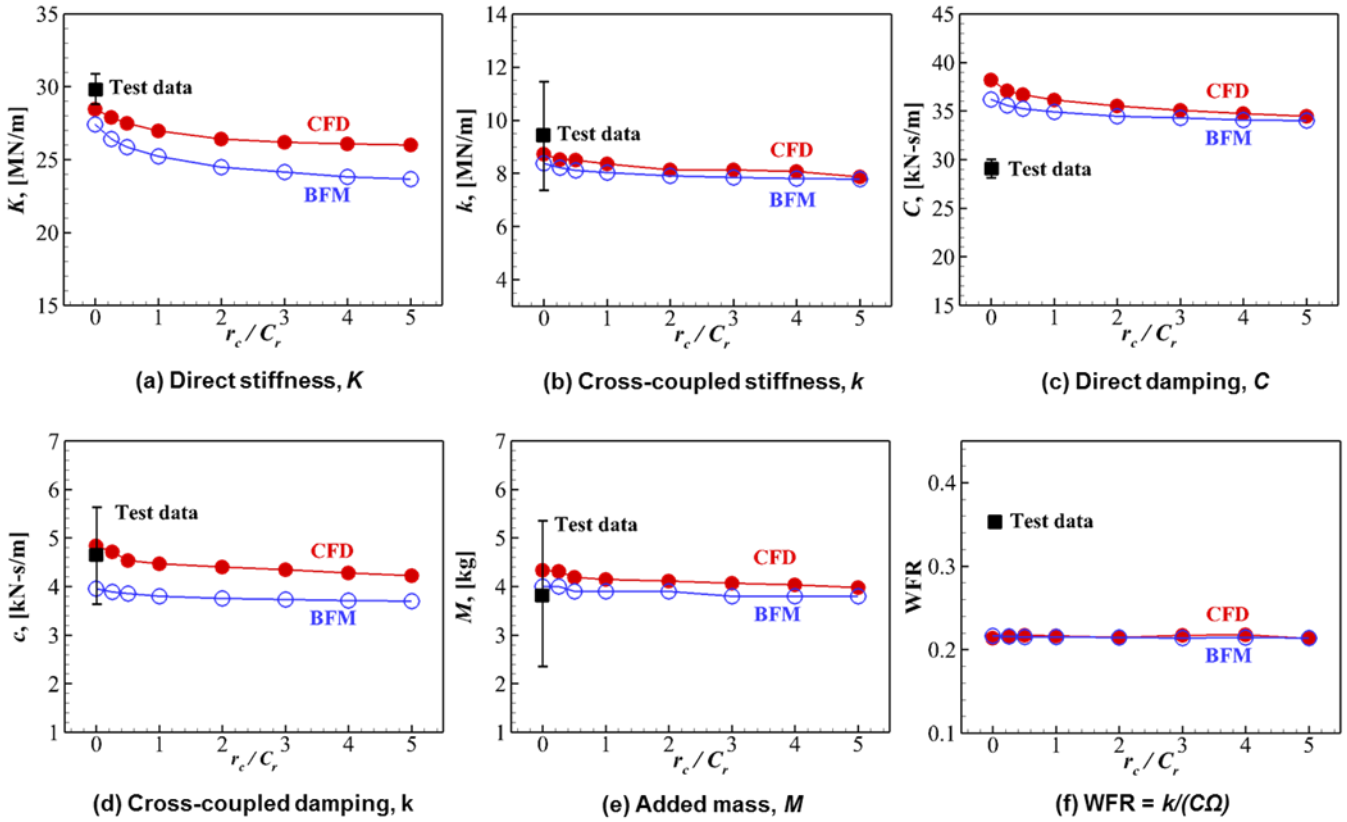

Fig. 10 Predicted seal rotordynamic force coefficients vs. inlet corner radius (r_c/C_r): (a) direct stiffness K; (b) cross-coupled stiffness k; (c) direct damping C; (d) cross-coupled damping c; (e) inertia M; and (f) WFR. Water annular seal (L/D = 0.46, C_r = 0.11 mm): 6.89 MPa pressure drop and rotor speed of 10,200 rpm. Test data from Marquette et al. (1997).

NOMENCLATURE

C_r	Seal radial clearance [m]
C, c	Direct and cross-coupled damping coefficients [Ns/m]
D	$2R$. Rotor diameter [m]
$F_{\bar{X}}, F_{\bar{Y}}$	Seal reaction force components (radial and tangential) [N]
K, k	Direct and cross-coupled stiffnesses [N/m]
L	Seal land length [m]
L_u	Length of upstream section to seal inlet [m]
M	Direct mass coefficient [kg]
$\dot{m}$	Leakage (mass flow rate) [kg/s], $\dot{m} = \rho Q$
P	Pressure [Pa]
P_s, P_a, P_e	Supply, discharge and entrance pressures [Pa]
r	Rotor whirl orbit radius [m]
r_c	Curvature radius of inlet plane round corner [m]
R	Rotor radius [m]
Re_a, Re_c	Reynolds numbers, axial and circumferential, $\mathrm{Re}_a = (2\rho W C_r)/\mu$, $\mathrm{Re}_c = (2\rho\Omega R C_r)/\mu$
U_θ, W	Average (cross-film) circumferential and axial velocities [m/s]
X, Y, Z	Inertial coordinate system
$\bar{X}, \bar{Y}, \bar{Z}$	Rotating coordinate system
WFR	Whirl frequency ratio, $k/(C\Omega)$
α	Circumferential swirl ratio, $\alpha = U_\theta/(\Omega R)$
ΔP	Pressure drop [Pa], $\Delta P = P_s - P_a$
ξ	Entrance pressure loss coefficient, $(P_s - P_e) = \frac{1}{2}\rho\ (1 + \xi)\ W^2$
θ	Circumferential coordinate [rad]
μ	Fluid absolute viscosity [Pa·s]
ν	Kinematic viscosity [m^2/s], $\nu = \mu/\rho$
ρ	Density, [kg/m^3]
ω	Whirl frequency [rad/s]
Ω	Rotor angular velocity [rad/s]

Abbreviations

BFM	Bulk-flow model
CFD	Computational Fluid Dynamics

ACKNOWLEDGMENTS

Thanks to the Turbomachinery Laboratory for the financial support and to the Texas A&M University High Performance Research Computing for access to their resources, including CFD software (ANSYS Fluent®).

REFERENCES

[1] Childs, D. W., (2013), *Turbomachinery Rotordynamics with Case Studies*, Minter Spring Pubs., 1st ed., Chapter 7.

[2] Hirs, G., (1973), A Bulk-Flow Theory for Turbulence in Lubricant Films, ASME J. Tribol., **95**(2), pp. 137-145.

[3] San Andrés, L., (1991), Analysis of Variable Fluid Properties, Turbulent Annular Seals, ASME J. Tribol., **113**(4), pp. 694-702.

[4] Marquette, O. R., Childs, D. W., and San Andrés, L., (1997), Eccentricity Effects on the Rotordynamic Coefficients of Plain Annular Seals: Theory versus Experiment, ASME J. Tribol., **119**(3), pp. 443-447.

[5] Al-Qutub, A. M., Elrod, D. and Coleman, H. W., (2000), A New Friction Factor Model and Entrance Loss Coefficient for Honeycomb Annular Gas Seals, ASME J. Tribol., **122**(3), pp. 622-627.

[6] Benedict, R. P., Carlucci, N. A., and Swetz, S.D., (1966), Flow Losses in Abrupt Enlargements and Contractions, ASME J. Eng. Power, **88**(1), pp. 73-80.

[7] Bullen, P. R., Cheeseman, D. J., Hussain, L. A., and Ruffell A. E., (1987), The Determination of Pipe Contraction Pressure Loss Coefficients for Incompressible Turbulent Flow, Int. J. Heat Fluid Flow, **8**(2), pp. 111-118.

[8] Constantinescu, V. N., and Galetuse, S., (1976), Pressure Drop Due to Inertia Forces in Step Bearings, ASME J. Lubrication Tech., **98**(1), pp. 167-174.

[9] San Andrés, L., and Velthuis J. F. M., (1992), Laminar Flow in a Recess of a Hydrostatic Bearing, Tribol. Trans., **35**(4), pp. 738-744.

[10] Ha, T. W., and Choe, B. C., (2012), Numerical Simulation of Rotordynamic Coefficients for Eccentric Annular-Type-Plain-Pump Seal Using CFD Analysis, J. Mech. Sci. Technol., **26**(4), pp. 1043-1048.

[11] Arghir, M., and Frene, J., (2004), A Bulk-Flow Analysis of Static and Dynamic Characteristics of Eccentric Circumferentially Grooved Liquid Annular Seals, ASME J. Tribol., **126**(2), pp. 316-325.

[12] Migliorini, P. J., Untaroiu, A., Wood, H. G., and Allaire, P. E., (2013), A Computational Fluid Dynamics/Bulk-Flow Hybrid Method for Determining Rotordynamic Coefficients of Annular Gas Seals, ASME J. Tribol., **134**(2), pp. 022202.

[13] San Andrés, L., Wu, T., Maeda, H., and Tomoki, O., (2017), A Computational Fluid Dynamics Modified Bulk Flow Analysis for Circumferentially Shallow Grooved Liquid Seals, ASME Paper No. GT2017-63492.

[14] Grigoriev, B., Schmied, J., Fedorov, and A., Lupuleac, S., (2006), Consideration of the Pressure Entrance Loss for the Analysis of Rotordynamic Gas Seal Forces, Paper-ID 245, 7th IFTOMM Conference on Rotor Dynamics, Vienna, Austria, September 25-28.

[15] Elrod D. A., Childs D. W., and Nelson C. C., (1990), An Annular Gas Seal Analysis Using Empirical Entrance and Exit Region Friction Factors, ASME J. Tribol., **112**(4), pp. 196-204.

[16] ANSYS, (2013), ANSYS Fluent User's Guide 15.0, ANSYS Inc., Canonsburg, PA.

[17] Yang, J., and San Andrés, L., (2018), On the Influence of the Entrance Section on the Rotordynamic Performance of a Pump Seal with Uniform Clearance: a Sharp Edge vs. a Round Edge, Proc. of ASME Turbo Expo, Norway, June 11-15, ASME Paper No. GT2018-75414.